Research Report

2003-43T

Low-cost Current-Fed PMSM Drive System with Sinusoidal Input Currents

V. Nedic, T.A. Lipo*

International Rectifier Corporation
Automotive IC R&D
El Segundo, CA 90245

*Wisconsin Power Electronics and Research Consortium
University of Wisconsin
Madison, WI 53706

Work performed at WEMPEC sponsored by CPES.

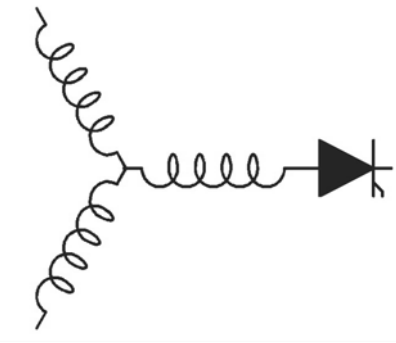

Wisconsin
Electric
Machines &
Power
Electronics
Consortium

University of Wisconsin-Madison
College of Engineering
Wisconsin Power Electronics Research Center
2559D Engineering Hall
1415 Engineering Drive
Madison WI 53706-1691

Low-Cost Current-Fed PMSM Drive System With Sinusoidal Input Currents

Velimir Nedić, *Member, IEEE*, and Thomas A. Lipo, *Fellow, IEEE*

***Abstract*—Standard low- and medium-power drives are based on the voltage-source converter topology. There has been less research work on dual topology drives, based on a current-fed inverter structure. Although energy storage is more efficient in capacitors than in inductors, due to some inherent advantages of current-source converter topology, and at the first place, the absence of a dc-link electrolytic capacitor, a current-source drive system made with a considerably reduced dc link inductor could be better low-cost solution with improved reliability, lifetime, and transient response than conventional drive.**

This paper is about a new current-fed drive topology with sinusoidal input currents, which is applied to a permanent-magnet synchronous machine in low-cost applications. A three-switch front-end pulsewidth modulator buck rectifier with an appropriate control technique, a simple thyristor inverter at the output, together with a small dc choke (which can be embedded in the machine), virtually offers an inductorless integrated drive system solution and could challenge standard industry solutions. System description, analysis, design guidelines, simulated results, and measured experimental results will be presented.

***Index Terms*—Current source, permanent-magnet motor, rectifier, self-controlled, thyristor.**

I. Introduction

OVER the last two decades, the traditional voltage-source inverter (VSI) topology with a diode rectifier—dc link capacitor—pulsewidth-modulator (PWM)-controlled inverter has become the preferred choice in ac drives for low-cost variable voltage and frequency power applications [1]. Although this drive system topology employs a simple diode front-end rectifier, it has been found to offer a very favorable performance/cost ratio.

Current-source converters have a number of inherent advantages that overcome some of the disadvantages common to voltage-source circuits [2]. The main advantage is the absence of a large electrolytic capacitor, which lowers the cost and increases the life span of the drive system. Furthermore, a current-source drive system made with a considerably reduced size of the dc-link inductor when compared with conventional current-source inverters (CSIs) could be a better low-cost solution with improved reliability, lifetime, and transient response than the VSI version.

Contrary to the current-source system topology, which is based on a three-phase thyristor rectifier on its input and PWM current-source inverter at the output [3], this paper describes the opposite drive topology structure, based on an integrated PWM three-switch three-phase buck rectifier [4]—minimized dc-link inductor—thyristor bridge configuration applied to a permanent-magnet synchronous machine (PMSM).

With a PWM rectifier at its input, sinusoidal input currents [5], [6], a suppressed dc link inductor drive system topology [7], [8], and a starting scheme based on chopped dc current is possible. It follows that the main advantages of the proposed approach for lower cost applications are the reduced number of fully controlled switches, elimination of the dc-bus capacitor, and the sinusoidal shape of the input phase currents. Moreover, the small dc choke can be embedded into machine creating virtually an inductorless drive system.

System description, analysis, design guidelines, simulated results, and measured experimental results will be presented in the following text. It will be shown how the three main problems associated with such a drive configuration, i.e., 1) sinusoidal control of the input currents in the presence of harmonic distortion on the dc link due to the six-step operation of the inverter; 2) operation with a small dc inductance; and 3) starting of the PMSM, are solved.

The paper is organized as follows: Section II presents a general description of the new integrated current-fed PMSM drive system solution proposed in this paper. A description of the developed rectifier charge-mode controller [9]–[11] and inverter starting technique are included as well; a system analysis such as commutation study and power-factor optimization are described in Section III; Section IV presents the simulated results obtained by using circuit simulator SABER and experimental data measured on the laboratory prototype. The description and the corresponding comments of the starting and steady-state operations of the drive system are given in this section.

II. Description of the System

A. Power Circuit Configuration

The block diagram of the proposed low-cost current-fed self-controlled PMSM drive system is shown in Fig. 1. The PMSM is fed from a load-commutated thyristor inverter supplied from a three-phase three-switch PWM buck rectifier through a very small dc-link inductor, which is virtually eliminated and

Paper IPCSD-05-067, presented at the 2003 Industry Applications Society Annual Meeting, Salt Lake City, UT, October 12–16, and approved for publication in the IEEE Transactions on Industry Applications by the Industrial Drives Committee of the IEEE Industry Applications Society. Manuscript submitted for review March 12, 2005 and released for publication February 24, 2006.

V. Nedić was with the Department of Electrical and Computer Engineering, University of Wisconsin, Madison, WI 53706 USA. He is now with Ancra International, Hawthorne, CA 90250 USA (e-mail: nedic@verizon.net).

T. A. Lipo is with the Department of Electrical and Computer Engineering, University of Wisconsin, Madison, WI 53706 USA (e-mail: lipo@engr.wisc.edu).

Digital Object Identifier 10.1109/TIA.2006.873667

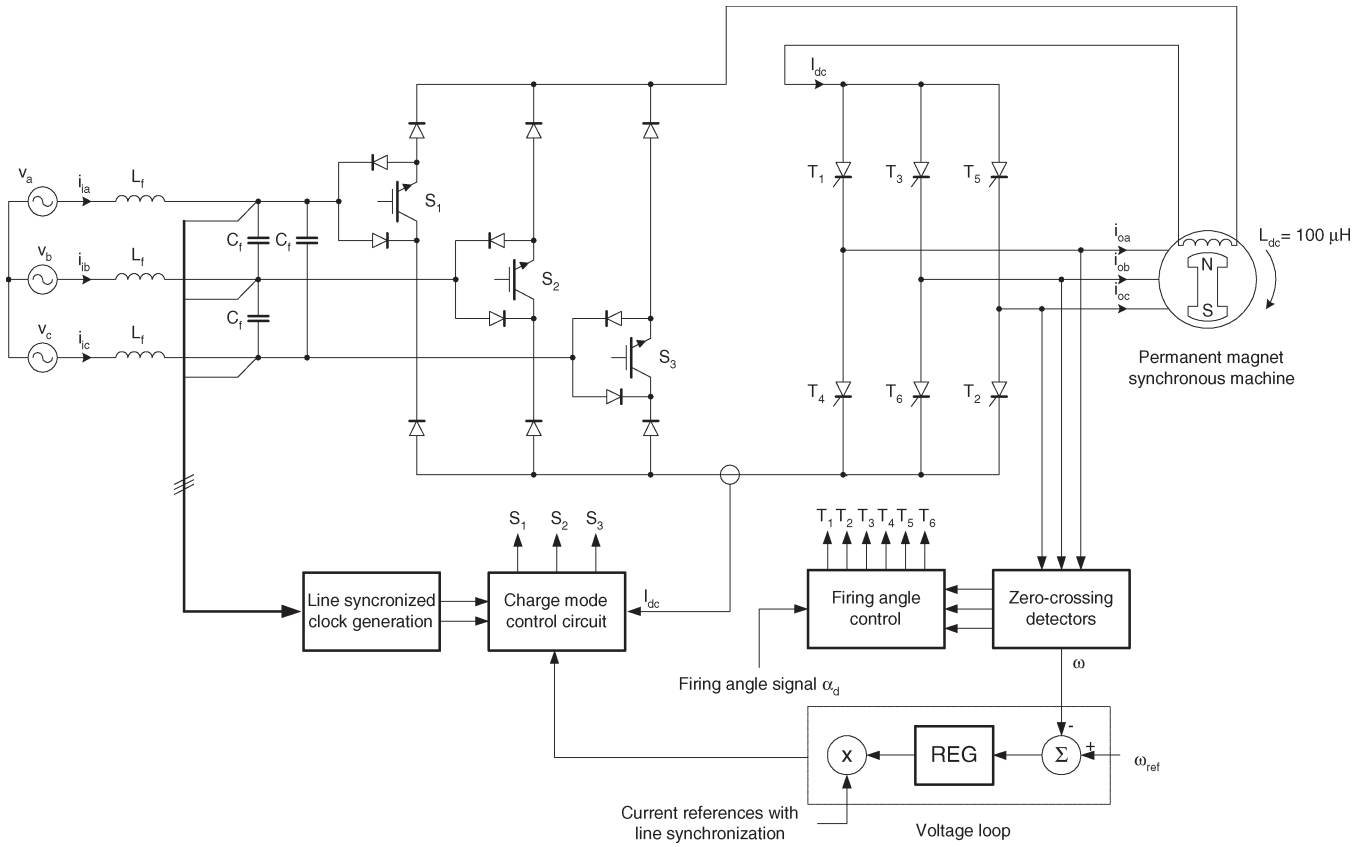

Fig. 1. Proposed low-cost PMSM drive. The load-commutated inverter is supplied from the three-switch PWM front-end rectifier through a very small dc-link inductor built in the machine.

embedded into the machine. As mentioned previously, the main reasons for using this power circuit configuration is to provide sinusoidal input currents, to control the load current when the smoothing dc-link inductor is very small, and to implement a simple starting scheme for the machine based on the interrupted dc link current.

The main function of the PWM rectifier is to regulate the level of the dc-link current and to provide sinusoidal currents at the input of the drive system. A small LC input filter easily absorbs the high-frequency harmonics injected into the ac mains by the rectifier switching action. It should be noted that although dc-link current contains a harmonic component at six times the inverter frequency, the rectifier controller enables sinusoidal modulation of the input currents.

The small dc-link inductor functions to smooth the dc link current and will be integrated into a new type of PMSM under development offering a virtually inductorless drive system. The magnitude of its inductance ($\approx 100\ \mu$H) is made as small as possible, under switching frequency limit and permissible dc-link current ripple (considering the iron losses and saturation conditions in the machine core).

Finally, the inverter consists of six thyristor switches operating in six-step mode, which are naturally commutated by the back electromotive force (EMF) induced in the machine during normal operation. This is the standard load-commutated inverter, serving as an electronic commutator, used in self-controlled synchronous machine drives [12]. Starting of the drive motor is achieved by interrupting the dc-link current prior to each commutation by proper gating of the PWM rectifier, so that the current freewheels to zero through one leg of the rectifier bridge.

The adopted control system configuration is depicted in Fig. 1. It is similar to standard control scheme for synchronous machine drives, but it employs only a speed control loop because current control is already included in the rectifier charge controller. It should be noted that motor speed sensing is not necessary because the speed feedback signal can be derived from the inverter synchronization signals. The complete control system uses only one sensor for the dc link current. Inverter triggering signals are synchronized to the rotor position by simple terminal voltage sensing instead of using position detectors. Therefore, an additional lowering of cost is achieved by implementing a position sensorless drive system, and, in addition, the machine power factor can be precisely controlled.

B. Charge Control of the Three-Switch PWM Rectifier

The three-phase step-down rectifier operation is based on the fact that the dc link inductor current is switched between the input phases such that the equivalent area per switching cycle reconstitutes a sine-wave current on that phase in the lower part of its harmonic spectrum. Therefore, to sinusoidally shape converter input currents, it is sufficient that they follow a given set of current references in an open-loop fashion. The best way to do this is to enable the average value of the input

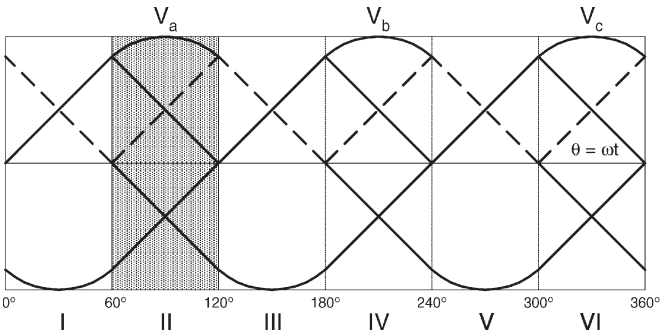

Fig. 2. Input phase voltages divided into six 60° sectors. The dashed and dotted lines represent modulating signals for each PWM during one line cycle.

TABLE I
RULES FOR IMPLEMENTING THE MODULATION ALGORITHM

		Sector in line cycle					
		I	II	III	IV	V	VI
Modulating laws	m_1	$\|V_a\|$	$\|V_b$	$\|V_b\|$	$\|V_c\|$	$\|V_c\|$	$\|V_a\|$
	m_2	$\|V_c\|$	$\|V_c$	$\|V_a\|$	$\|V_a\|$	$\|V_b\|$	$\|V_b\|$
Gate signals	S_a	$\|d_1\|$	1	$\|d_2\|$	$\|d_2\|$	1	$\|d_1\|$
	S_b	1	$\|d_1$	$\|d_1\|$	1	$\|d_2\|$	$\|d_2\|$
	S_c	$\|d_2\|$	$\|d_2$	1	$\|d_1\|$	$\|d_1\|$	1

current vectors to track its corresponding sinusoidal reference. Inasmuch as charge-mode control behaves as an instantaneous large-signal average current control of switching converters, it is therefore very suitable for average value control of a pulsating variable, such as the input phase currents of the three-phase buck rectifier.

In the drive system proposed in this paper, the objective is to decrease as much as it is possible the dc link inductor, and therefore, standard sinusoidal ramp-based PWM techniques are not suitable for control as they require a large output inductor to reduce the output current switching ripple. Furthermore, the dc current will exhibit triple harmonic distortion due to the six-step operation of the output inverter. The assumption was that with charge control, the low input current distortion should be achieved even with large current ripple at the dc output because the input currents would follow the sinusoidal current references during each switching cycle.

The adopted modulation scheme is a six-step discontinuous algorithm, which resembles the natural operation of the three-phase buck rectifier, offers minimum switching action, and is simple to realize. According to this technique, a line cycle is divided into six sectors, each of 60°, as shown in Fig. 2.

In each sector, due to the presence of the diodes and relative polarity of the input voltages, the switch in the phase corresponding to the maximum absolute voltage is kept on during entire 60° interval without affecting the circuit performance. This simplifies control strategy and reduces switching losses. The switches in the other two phases with opposite sign are pulse-modulated, according to the modulation laws, which are proportional to the associated phase voltages. The switching rules are summarized in Table I.

The designed charge-mode controller employs two current references and two charge-mode PWM comparators to produce two necessary independent duty cycles at any instant, as shown in Fig. 3. Inasmuch as the switch currents drawn from the corresponding input phases are in turn dc-link current, it is enough to sense only the dc inductor current to depict switch current information at any time. Note that the PWM generator is realized as a center-aligned switching scheme. Instead of having one freewheeling period at the end of each switching cycle, it is proportionally distributed between two nonzero duty cycles, which minimizes peak-to-peak dc current-switching ripple. To accomplish this, two 180° phase-shifted clock signals CLK_1 and CLK_2 are used.

C. Inverter Starting Scheme

At startup and at low speeds, some type of forced commutation is required to commutate the inverter to start and accelerate the motor until the machine terminal voltages are sufficiently large to ensure reliable commutation. The forced current commutation between inverter thyristors without any additional power circuit components can be accomplished by periodically interrupting the dc-link current. That is, the dc link current is forced to become zero prior to each commutation by proper gating of the PWM rectifier, thus providing the turn-off of outgoing thyristors. When the dc link current drops to zero, commutation of the thyristor in the inverter bridge is enabled. Natural commutations begin when machine reaches speed at which induced back EMFs are large enough to ensure safe commutation.

Zero-current intervals on the dc link are accomplished simply by disabling charge controller of the rectifier at each change of the phase-reference signals. The startup pulse is then generated and passed to the rectifier controller resetting both PWM charge modulators, as shown in Fig. 3. Active duty cycles d_1 and d_2 become then zero, and the dc link current freewheels and decreases to zero through the third switch, which is normally on during the corresponding 60° sector, according to the six-step PWM control principle. The width of disabling pulse is set to ensure required length of the zero-current intervals on the dc link and reliable commutation.

D. Low-Cost Issues

The inspiration to use load-commutated thyristor inverter for driving PMSM comes from the low-cost requirements of the target applications. Almost all of the applications, such as high-voltage ac (HVAC) drives, home appliances, fans, pumps, etc., do not require precise positioning or speed control, and a load-commutated PMSM drive could be a strong competitor [13]. The idea is to use a fully controlled converter at the front end to supply a self-controlled PMSM enabling minimization of the dc link inductor, a simple starting scheme, and sinusoidal input currents. The relatively small dc inductance could be embedded into the machine offering a new low-cost integrated drive solution, which is virtually without any link components.

Inasmuch as low cost does not have to mean low performance, the system specifications and drive characteristics have to be justified with the price of the equipment. It has been shown that the benefits of using the proposed drive configuration are improved input characteristics while keeping system

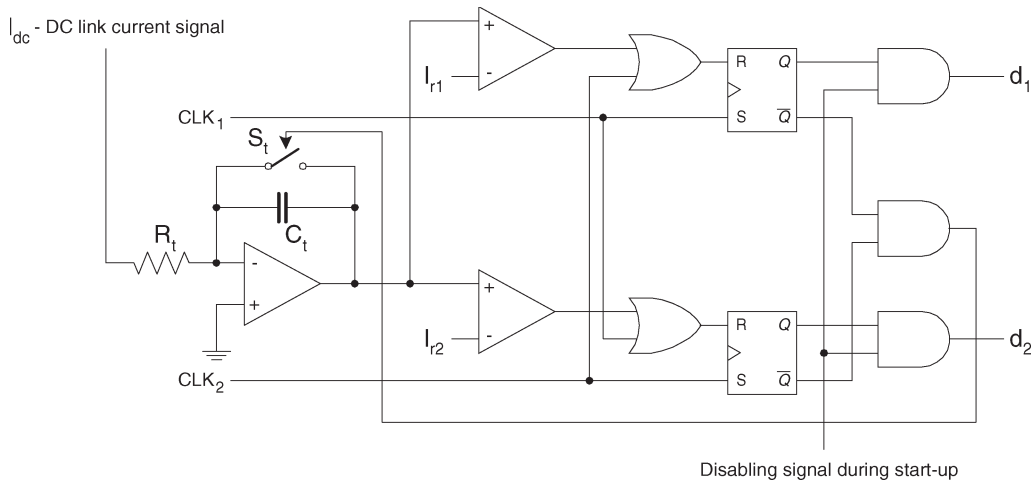

Fig. 3. Implemented charge-mode controller. It uses two clock signals CLK_1 and CLK_2 to generate center-aligned PWM scheme. The zero duty cycle is distributed between two active duty cycles d_1 and d_2.

simplicity. The expense of use of fully controlled switches is acceptable because there are only three of them and benefits are improved power quality. Compared to conventional VSI drive, the combination of three switches and 12 diodes costs much less than combination of six switches and six diodes. Furthermore, a bulky and expensive dc link capacitor can be eliminated. Instead, a small inductor is employed with potential of its total elimination.

The price to pay is increased torque oscillations and incapability of precise position control [14]. However, the attractiveness of simplicity and the reliability of a load-commutated inverter overcome its potential lower performance in many target applications. Mostly, such inverter–machine combinations have become the preferred solution at higher power ratings due to the availability of high-current thyristor devices. However, the use of thyristor inverters in HVAC applications where power requirements are in the order of several horse powers is also possible because today's thyristor are much cheaper than fully controllable switches of the same power rating. Therefore, improved system performance, reliability, and reduced component count can be achieved.

III. System Analysis

A. Commutation Analysis

Commutation in a self-controlled PMSM is a complex process that depends on the load current and the machine voltage (which is a function of the machine speed) for a given firing angle. In a natural commutation process, the current always leads the voltage, and the machine power factor is determined by the phase angle between the inverter triggering pulses and the machine voltage. Thus, to maximize the machine power factor, it is necessary to maintain the inverter firing angle β at a minimum permissible value, which can be expressed as

$$\cos\beta = \cos(\omega t_q) - 2L_c\frac{\omega}{V_{\mathrm{ll}}}I_{\mathrm{dc}} \tag{1}$$

where t_q is thyristor turn-off time. However, the above equation is based on an ideally smooth dc-link current and an infinite dc link inductance. In the presented drive system, the objective is to reduce as much as possible the energy storage on the dc link. With a small dc-link choke and having the PWM rectifier at the input of the drive system, the switching ripple is reflected to the machine voltages, and consequently, the voltage across the thyristors contains switching ripple distortion, which effectively decreases available margin angle [15]. The smaller the dc inductance, the higher the switching ripple is across the machine inductances and thyristors.

In other words, the voltage difference between the dc-link voltage V_{dc} and line-to-line machine voltage V_{ll} is divided up on both the inductances L_{dc} and L_c, depending on their ratio, L_{dc}/L_c. For decreasing L_{dc}, this voltage drop appears primarily on L_c. Therefore, the motor and thyristor voltages are composed of the sinusoidal voltage and the voltage drop on the machine leakage inductance, which is pulsating with the rectifier switching frequency. The equation for voltage across the thyristor V_{Th}, following its turn-off, can be obtained as

$$V_{\mathrm{Th}} = V_{\mathrm{ll}}\sin(\omega t-\beta) + \frac{V_{\mathrm{dc}} - V_{\mathrm{ll}}\sin\left(\omega t-\beta+\frac{\pi}{3}\right)}{2+\frac{L_{\mathrm{dc}}}{L_c}} \tag{2}$$

and it can be calculated analytically as follows. Applying a Fourier analysis approach, the rectifier switching functions can be represented by the corresponding Fourier series as

$$\begin{aligned} h_a(t) &= m_a + \frac{2}{\pi}\sum_{n=1}^{\infty}\frac{\sin(\pi n m_a)}{n}\cos\left(\frac{2\pi n t}{T}\right) \\ h_b(t) &= m_b + \frac{2}{\pi}\sum_{n=1}^{\infty}\frac{\sin(\pi n m_b)}{n}\cos\left(\frac{2\pi n t}{T}\right) \\ h_c(t) &= m_c + \frac{2}{\pi}\sum_{n=1}^{\infty}\frac{\sin(\pi n m_c)}{n}\cos\left(\frac{2\pi n t}{T}\right) \end{aligned} \tag{3}$$

where m_a, m_b, and m_c are the modulation indexes for each rectifier phase. The above equations allow calculation of the output waveforms of a switching converter structure by applying the superposition principle of the converter's response on each Fourier frequency harmonic excitation. Therefore, assuming

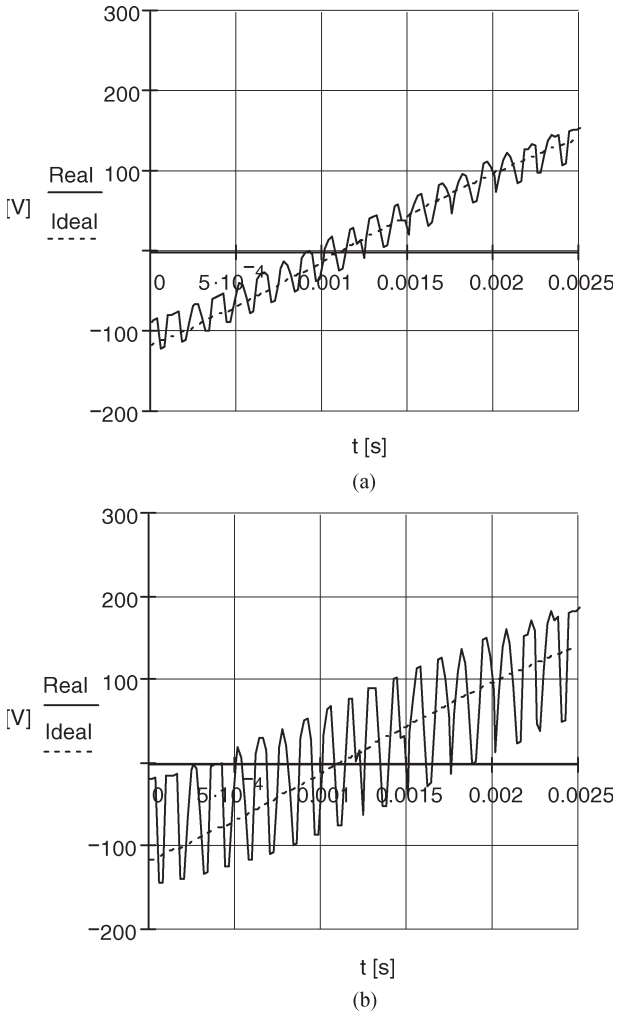

Fig. 4. Plots of the voltage waveform $V_{\rm Th}$ across thyristor upon its turn-off for firing angle $\beta = 50^\circ$ and $L_c = 1$ mH for two different values of $L_{\rm dc}$. (a) $L_{\rm dc} = 5$ mH. (b) $L_{\rm dc} = 100$ μH.

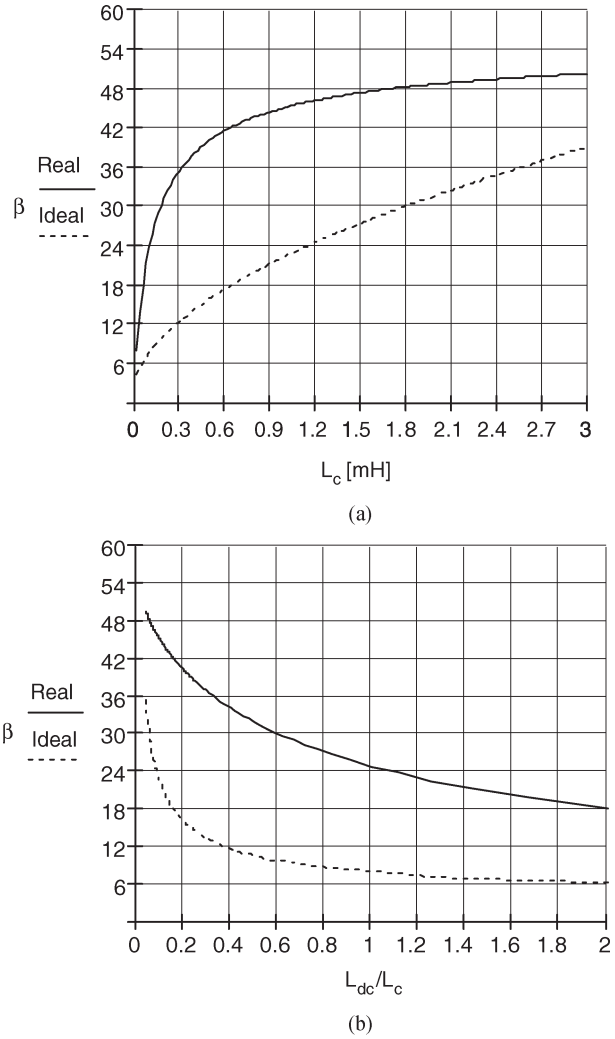

Fig. 5. Plots of the necessary inverter firing angle β at speed $n = 1500$ r/min and for dc link current $I_{\rm dc} = 10$ A. (a) As a function of machine leakage inductance L_c. (b) As a function of ratio $L_{\rm dc}/L_c$.

the symmetric input phase voltages, the dc-link voltage can be calculated from

$$V_{\rm dc} = h_a v_a + h_b v_b + h_c v_c \tag{4}$$

and applied in (2) to calculate the thyristor voltage. The results for one thyristor are shown in Fig. 4(a) and (b) for two different values of dc link inductance $L_{\rm dc}$. The firing angle used in calculations equals $\beta = 50^\circ$, and the value of the machine leakage inductance is $L_c = 1$ mH. The instant $t = 0$ on the graphs corresponds to the turn-off of a thyristor. The dotted traces show the voltage across thyristor when $L_{\rm dc}$ is assumed to be infinite, and the solid traces represent the calculated thyristor voltage for the specified $L_{\rm dc}$. One can note that the thyristor voltage waveform follows the envelope of the machine back EMF, but it contains the switching ripple as well, which considerably decreases the margin angle when $L_{\rm dc}$ is decreasing to $L_{\rm dc} = 100$ μH, as demonstrated in Fig. 4. Hence, the inverter firing angle β may have to be increased until the negative blocking voltage during the recovery time is reached.

Inasmuch as the switching pattern of the rectifier is independent of the inverter operation, the influence of the decreasing ratio $L_{\rm dc}/L_c$ on the machine-commutated inverter is analyzed upon the upper envelope of the thyristor voltage high-frequency ac component, which can be calculated from (2) for a specified constant value of the dc link voltage. The thyristor voltage should be negative following the commutation to achieve proper blocking capabilities, and assuming the minimum required recovery time is $t_q = 100$ μs and the worst case situation where the maximum line-to-line input ac voltage appears on dc link $V_{\rm dcmax} = 325$ V, the necessary inverter firing angle as a function of the machine leakage inductance is calculated.

The results are presented in Fig. 5(a) and (b), which show the required inverter firing angle calculated from dotted trace and solid trace for $n = 1500$ r/min and $I_{\rm dc} = 10$ A. It can be seen that the inverter firing angle has to be increased, compared with an ideal case with infinite inductance, until the negative blocking voltage across the thyristor is reached to ensure proper operation of the drive system. Fig. 5(b) shows the same

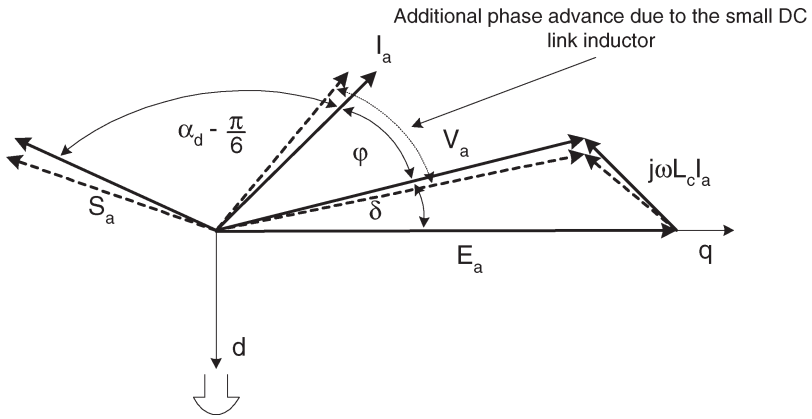

Fig. 6. Phasor diagram of the PMSM supplied by the load-commutated inverter. Due to the small dc-link inductor, the phase difference between machine voltage and current is increased.

traces but versus ratio $L_{\rm dc}/L_c$, which demonstrates that the smaller the machine leakage inductance, the smaller the inverter firing angle.

B. Power-Factor Optimization

Although the proposed self-commutated PMSM drive has a simple configuration and high availability, it must operate at a leading power factor because only then can the machine back EMF commutate the thyristors. Thus, the machine cannot operate in the maximum torque per ampere region. Furthermore, the analysis from the previous section indicates the loss of available mechanical power due to the effect of the decreasing margin angle with small dc-link inductor. Consequently, a decrease of the dc link inductance affects the power factor of the machine as indicated by the machine vector diagram in Fig. 6 because thyristor firing has to be additionally advanced, thus inverter firing angle is increased to ensure reliable thyristor commutation.

The machine power factor in the described system can be approximately calculated from the phase difference between the inverter firing angle and commutation angle as

$$\text{PF} = \cos\phi \approx \cos\left(\beta - \frac{\mu}{2}\right). \tag{5}$$

To optimize the power factor and achieve minimum reactive current loading of a machine–converter system, it is necessary to maintain the inverter firing angle at a minimum permissible value and operate the inverter at its commutation limit, as mentioned.

Equation (5) can be used to plot the machine power factor as a function of the machine leakage inductance L_c. Fig. 7(a) shows the machine power factor calculated assuming an infinite dc link inductance (dotted trace) and for $L_{\rm dc} = 100$ μH (solid trace) at $n = 1500$ r/min and $I_{\rm dc} = 10$ A. Fig. 7(b) represents the same traces but versus ratio $L_{\rm dc}/L_c$, which demonstrates that the smaller the machine leakage inductance, the higher the obtainable power factor.

By comparing the traces in Fig. 7, it can be noted that the available power factor is additionally decreased. In other words, due to the necessary increase in firing angle, the power factor has to be sacrificed to provide safe commutation. This

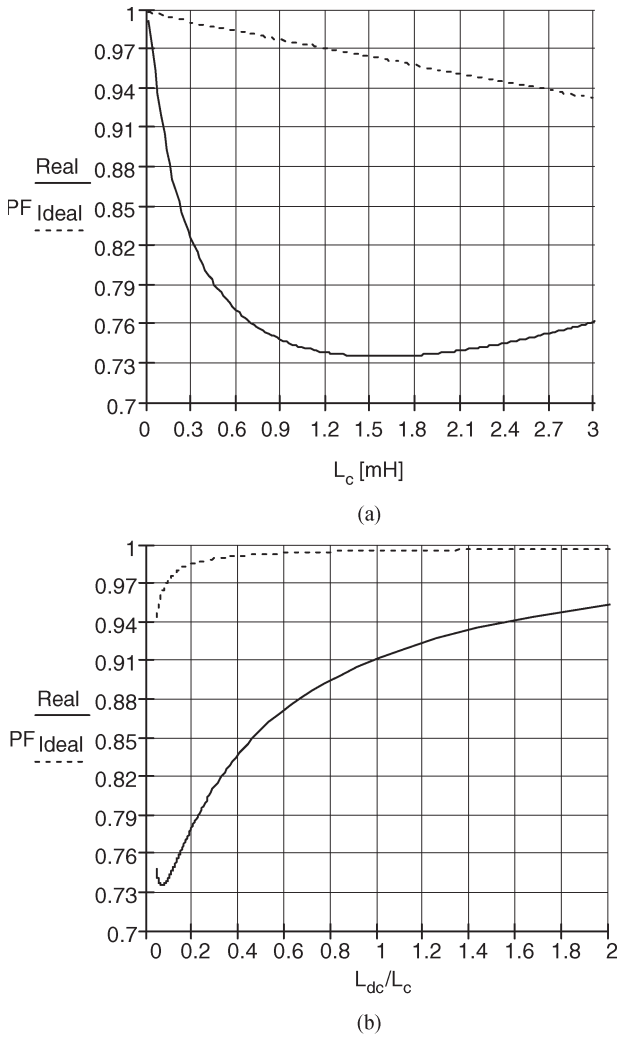

Fig. 7. Plots of the machine power factor at speed $n = 1500$ r/min and for dc-link current $I_{\rm dc} = 10$ A. (a) As a function of machine leakage inductance L_c. (b) As a function of ratio $L_{\rm dc}/L_c$.

may seem to be an important disadvantage because the load-commutated inverter is controlled at its commutation limit to ensure minimum reactive power loading of the motor–converter system. It should be also mentioned that the increase of power

factor with increasing machine leakages after its initial drop represents the fact that with increasing machine leakage inductance, the overlap angle increases as well, effectively reducing the phase difference between machine voltage and current.

Therefore, it is shown that smaller machine leakage inductance allows operation of the load-commutated inverter with a higher power factor in the presence of a smaller dc link inductance. The voltage difference between the dc link voltage and line-to-line machine voltage is distributed more evenly on the inductances $L_{\rm dc}$ and L_c in that case, making the necessary increase of the inverter firing angle due to the small dc link inductance smaller. However, note that there is a certain region for small machine leakage inductance where this improvement is not recognizable. This is due to the initial steep increase of the firing angle requirements due to the small dc-link inductance. Then, it stays more consistently on a value defined by the operating conditions where, as mentioned, with increasing machine leakage inductance, the power factor is improved due to the effective reduction of the phase difference between the machine voltage and current.

On the other side, higher machine leakage inductance is desired from the point of view of smoothing the dc link current ripple because it is effectively added to the dc-link inductor, allowing smaller input filter components. Therefore, a tradeoff in operating the drive system exists depending on the actual machine parameters and the desired size of the dc link inductance. Assuming that the rectifier output filter is rated only to limit ripple due to the modulation, the following equation may be used to evaluate the size of the dc-link inductance:

$$L_e = \frac{\sqrt{3}V_m}{4f_s\Delta I} \tag{6}$$

where $L_e = L_{\rm dc} + 2L_c$ is the total equivalent rectifier filter inductance composed of the dc link inductance $L_{\rm dc}$ and twice the machine leakage inductance L_c, V_m is the amplitude of the input phase voltage, ΔI is the permissible current ripple, and f_s is the PWM carrier frequency. To take a design example, assume that the maximum permissible ripple in the dc link current is limited to 50% of the rated current, that is, $\Delta I = 5$ A and $f_s = 7680$ Hz. Then, total equivalent inductance should be bigger than $L_e = 2.1$ mH. This means that, for $L_{\rm dc} = 100$ μH, the machine leakage inductance should be bigger than 1 mH.

Based on the above analysis, a machine leakage inductance within the range of 1–4 mH seems to be an optimum for this drive system configuration. The upper boundary of this range is increased for lower speed machines, that is, for machines with a higher back-EMF constant. The lower range boundary is extended for machines with a lower back-EMF constant.

It should be noted that the decrease of effective margin angle due to the switching ripple in the machine voltages is worse with increasing switching frequency. Thus, another benefit of using charge control of the PWM rectifier arises because it permits operation with fairly low switching frequency, making the additional necessary increase of the inverter firing angle smaller. Furthermore, in that way, the core losses in the machine are reduced, preventing the saturation of the machine core with an integrated dc link inductance structure.

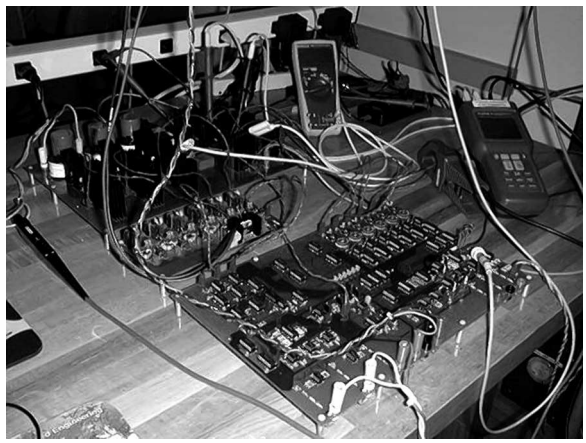

Fig. 8. Experimental prototype of the low-cost drive system.

IV. Simulated and Experimental Results

The operation of the complete system was simulated to investigate and demonstrate the feasibility of the proposed drive system. Simulated waveforms were obtained by using the circuit simulation package SABER. It is assumed that drive system is supplied from a three-phase 230-V root-mean-square (rms) line-to-line ac system. The frequency of the triangular clock carriers is set to 7680 Hz, that is, multiple of the line frequency, which is useful for synchronization in the hardware implementation.

To simulate the drive machine, the SABER built-in model for a PMSM was used. The machine parameters are given in the Appendix and correspond to a commercially available motor made by BEI Kimco used in the experiment. The motor is fan-loaded, typical for pump applications.

To experimentally verify the proposed power conversion concept and to confirm the correctness of the analytical and simulated results, a 3-kW laboratory prototype has been fabricated. The experimental prototype is rated for 10 A and is supplied from 230-V ac mains. Fig. 8 shows the photograph of laboratory prototype.

The experiments were carried out in a way to determine the possible limits of decreasing the dc-link inductance. Inasmuch as simulations have shown that it is possible to integrate an inductance of 100–200 μH into the machine core, the dc-link inductance was gradually decreased, and the waveforms, which will be shown in the next section, correspond to the operation with 100 μH on the dc link.

Fig. 9(a) and (b) shows the simulated and experimentally measured waveforms of the input current and the dc link current of the proposed drive system during the starting operation. From figures, it can be seen that the zero-current intervals on the dc-link current (bottom trace) are reflected in the input current (top trace) as notches, but these distortions last only during startup operation. As described before, the dc-link current is interrupted by the control startup signal to enable the zero-current intervals required for thyristor commutation. The experimental waveforms confirm that the starting scheme is successful and can be used to accelerate the drive motor.

The simulated and experimental waveforms of the input phase current and voltage and the dc link current under

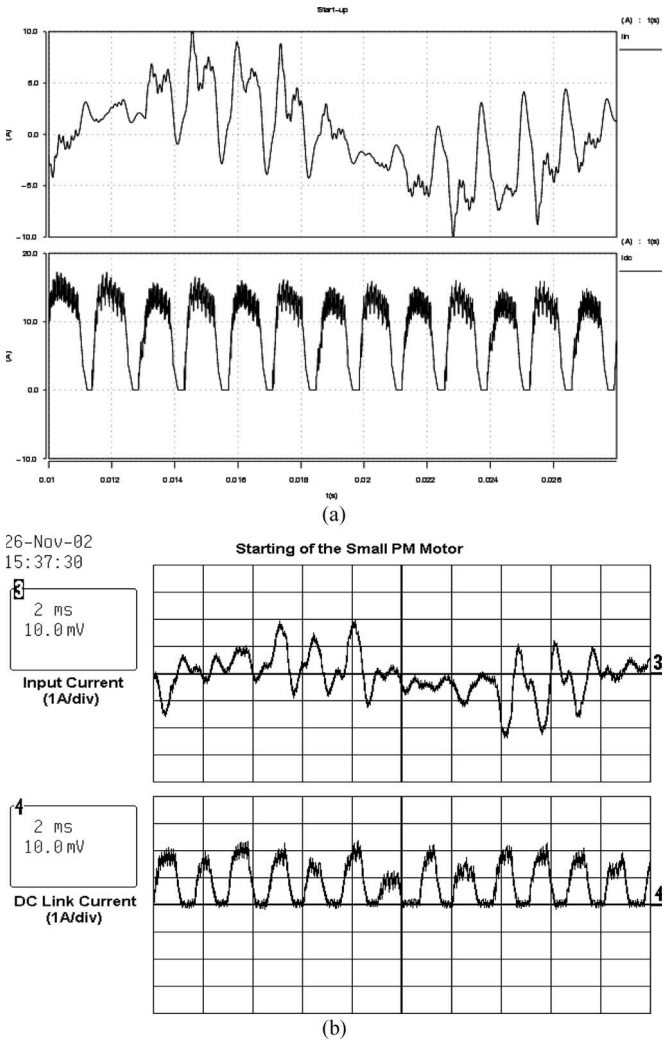

Fig. 9. Simulated and experimental waveforms during the starting operation. The top trace is input phase current (scale 1 A/div), whereas the bottom trace is dc-link current (scale is 1 A/div).

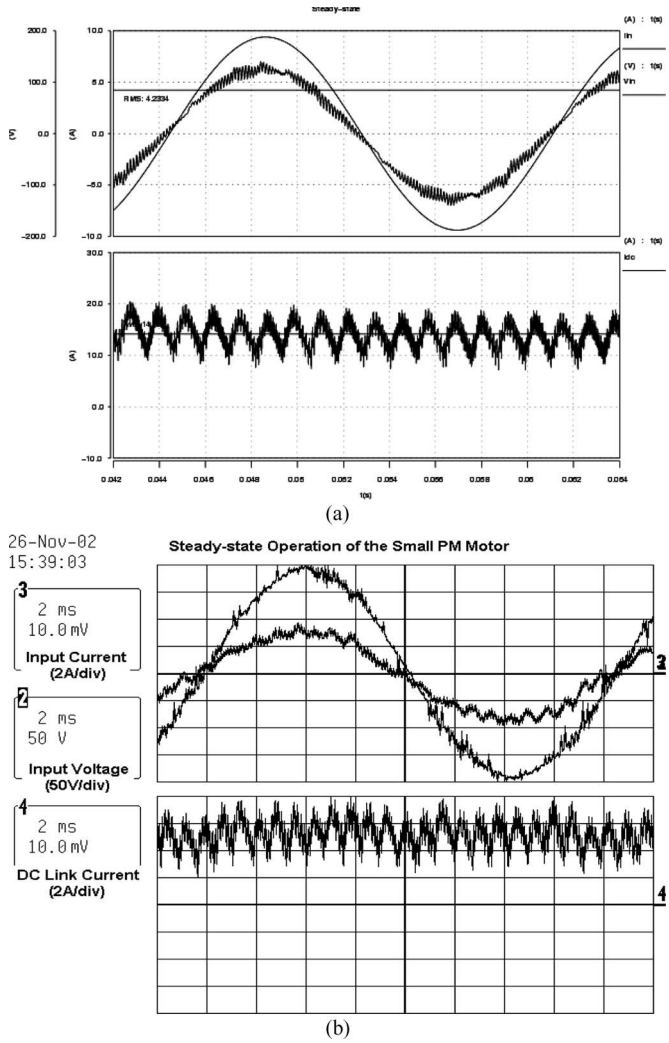

Fig. 10. Simulated and experimental waveforms of steady-state operation. The bottom trace is dc-link current (scale is 2 A/div), whereas the top trace is input phase current (scale is 2 A/div) and voltage (50 V/div).

steady-state operation are shown in Fig. 10(a) and (b). Referring to Fig. 10, although the dc link current (bottom trace) contains harmonic distortion due to the six-step operation of the inverter bridge and rectifier switching, the input phase current (top trace) is sinusoidally shaped with the low-frequency harmonic components being suppressed substantially while shifting the unwanted harmonic components near the switching frequency. These unwanted high-frequency components are filtered out by the LC input filter components. Also, it can be seen that the synchronization circuitry with simple phase shifting of the voltage synchronization signals works well, and input displacement factor is unity.

The steady-state waveforms of the output current and the thyristor voltage during one cycle of the output excitation frequency are shown in Fig. 11(a) and (b). The machine operating speed in this figure is 3900 r/min, and the power factor is about 0.77. Referring to Fig. 9, it is clear that the output current has a quasi-square waveform containing many harmonics because the dc link current is distorted due to operation with a very small dc link choke. The machine torque is consequently affected, containing ripple due to the six-step operation and switching action, but for certain application, this distortion is tolerable.

At this point, it is useful to comment on tradeoffs of the proposed drive system. As mentioned before, the higher machine leakage inductance is desired from the point of view of smoothing the dc link current and in obtaining higher quality input current waveforms. However, for higher machine leakage inductance, it is required to operate at a higher inverter firing angle to achieve safe and reliable thyristor commutation. Consequently, the power factor is reduced and available power is sacrificed. However, one should keep in mind that this is only true until the power factor reaches its minimum as shown in Fig. 8. After that point, there is a region where the power factor naturally increases as a result of the increasing overlap angle, with increasing leakage inductance. Although the attainable power factor is reduced compared with operation with a large dc link inductor, this region is probably more desired because much better input currents result.

It is important to analyze the loss of available power when operating the proposed drive system. Assuming the operating conditions from Figs. 9–11 and using the analytical equations

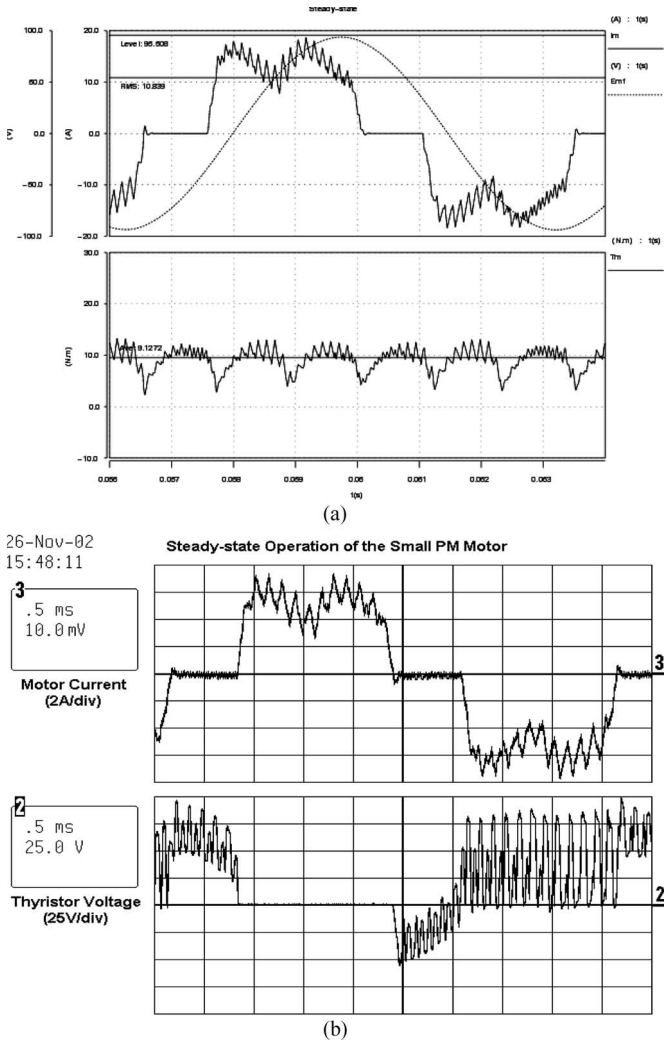

Fig. 11. Simulated and experimental waveforms of steady-state operation. The bottom simulated trace is machine torque, whereas the bottom experimental trace is thyristor voltage (scale 25 V/div); the top trace is motor phase current (scale 2 A/div) in both figures.

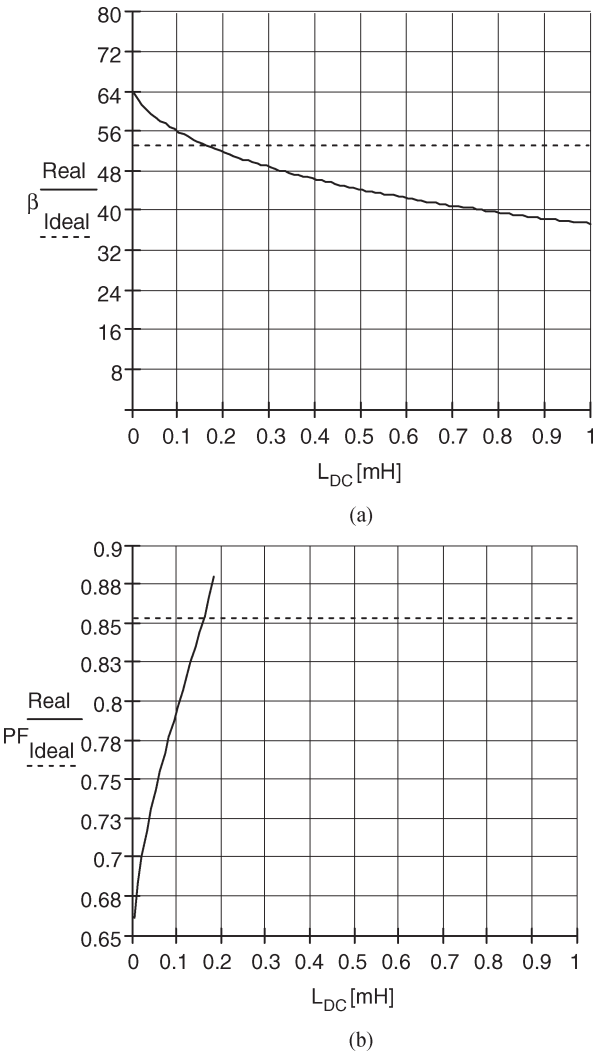

Fig. 12. Plots of the necessary inverter firing angle β and machine power factor. (a) Inverter firing angle as a function of dc-link inductance. (b) Power factor as a function of dc-link inductance.

from Section III, the necessary inverter firing angle and resulting power factor are calculated as a function of the dc link inductance. The results are shown in Fig. 12(a) and (b) for an infinite dc link inductance (dotted traces) and for varying dc link inductance (solid traces). As can be seen, when operating the proposed drive system with $L_{\rm dc} = 100$ μH, the machine must be derated at about 7% of the maximum attainable power. Furthermore, for dc-link inductance values above 200 μH, the machine can be operated as if an infinite dc-link inductance was present.

V. Conclusion

A new current-source drive topology for supplying a PMSM has been presented in this paper. The main idea was to use a drive topology structure with a PWM three-phase buck rectifier at its input and to supply a PMSM with a simple load-commutated thyristor inverter. The motivation of such an approach is that it makes it possible to minimize the smoothing dc inductor and potentially integrate it into a new type of machine under development. In addition, having a PWM rectifier as the front-end unit in utility interfaced systems offers benefits such as improved quality of power drawn from the ac system and sinusoidally shaped input currents. The poorer output drive characteristics due to the six-step inverter operation and incapability of precise positioning and speed control are justified because the drive system is intended to be used in low-cost HVAC applications or the appliance industry.

Simulated and experimental results have confirmed the feasibility of the proposed power conversion scheme. The operation of the proposed drive system employing a considerably low dc inductance is possible because the machine leakage inductances are utilized to smooth the dc link current. The starting scheme based on interrupted dc link current is efficient and does not require a complicated control implementation. The drawback of such a configuration is lower machine power factor operation because the inverter firing angle has to be increased to ensure safe thyristor commutation in the presence of reduced energy storage on the dc link. However, this loss of the available power is not critical, and it depends on the desired drive characteristics and machine used.

The main advantages of the proposed approach for lower cost applications are reduced number of fully controlled switches, significant reduction of the energy storage on the dc link and complete elimination of the bulky dc bus capacitor compared with standard VSI-based drive topologies, simpler and more efficient drive configuration than a conventional VSI driving induction motor, and sinusoidal shape of the input phase currents. Furthermore, by using the PMSM with an integrated dc link inductance, the drive system becomes virtually inductorless. Therefore, it can be said that the proposed drive topology achieves certain performance/cost advantages over voltage-source drive systems for low-cost applications. It is a new integrated drive system solution that could challenge the standard industry solutions for low-cost applications.

APPENDIX
MOTOR PARAMETERS

- Number of poles: 8;
- torque sensitivity: 0.167 N · m/A;
- back EMF constant: 0.167 V/rad/s;
- winding resistance: 0.69 Ω;
- winding inductance: 1.8 mH;
- rotor inertia: 2.66×10^{-4} kg · m^2.

REFERENCES

[1] T. J. E. Miller, *Brushless Permanent-Magnet and Reluctance Motor Drives*. Oxford, U.K.: Clarendon, 1989.

[2] D. W. Novotny and T. A. Lipo, *Vector Control and Dynamics of AC Drives*. Oxford, U.K.: Clarendon, 1996.

[3] B. Wu, S. B. Dewan, and G. R. Slemon, "PWM–CSI inverter for induction motor drives," in *Conf. Rec. IEEE-IAS Annu. Meeting*, 1989, pp. 508–513.

[4] L. Malesani and P. Tenti, "Three-phase AC/DC PWM converter with sinusoidal AC currents and minimum filter requirements," *IEEE Trans. Ind. Appl.*, vol. IA-3, no. 3, pp. 71–77, Jan./Feb. 1987.

[5] D. J. Tooth, S. J. Finney, and B. W. Williams, "Effects of using DC-side average current-mode control on a three-phase converter with an input filter and distorted supply," *Proc. Inst. Elect. Eng.—Electr. Power Appl.*, vol. 147, no. 6, pp. 459–467, Nov. 2000.

[6] N. R. Zargari and G. Joos, "A current-controlled current-source type unity power factor PWM rectifier," in *Conf. Rec. IEEE-IAS Annu. Meeting*, 1993, pp. 793–799.

[7] P. D. Ziogas, Y. Kang, and V. R. Stefanović, "Rectifier-inverter frequency changers with suppressed dc link components," *IEEE Trans. Ind. Appl.*, vol. IA-22, no. 6, pp. 1027–1036, Nov./Dec. 1986.

[8] J. Holtz and U. Boelkens, "Direct frequency converter with sinusoidal line currents for speed-variable ac motors," *IEEE Trans. Ind. Electron.*, vol. 36, no. 4, pp. 475–479, Nov. 1989.

[9] K. M. Smedley and S. Ćuk, "One-cycle controlled of switching converters," in *Proc. IEEE PESC*, 1991, pp. 887–896.

[10] K. Wang, D. Borojević, and F. C. Lee, "Charge control of three-phase buck PWM rectifiers," in *Proc. IEEE APEC*, 2000, pp. 824–831.

[11] C. Qiao and K. M. Smedley, "One-cycle controlled three-phase buck-derived rectifier," in *Proc. IEEE Power Electron. Motion Control Conf.*, 2000, pp. 430–435.

[12] H. Le-Huy, A. Jakubowicz, and R. Perret, "A self-controlled synchronous motor drive using terminal voltage sensing," in *Conf. Rec. IEEE-IAS Annu. Meeting*, 1980, pp. 411–418.

[13] S. P. Waikar, H. A. Toliyat, A. S. Ba-Thunya, Z. Zhang, and J. C. Moreira, "A novel thyristor-based brushless DC motor drive for low-cost applications," in *Proc. IEEE APEC*, 2001, pp. 434–439.

[14] T. M. Jahns, "Torque production in permanent-magnet synchronous motor drives with rectangular current excitation," *IEEE Trans. Ind. Appl.*, vol. IA-20, no. 4, pp. 139–145, Jul./Aug. 1984.

[15] J. C. Bendien and J. Geuenich, "On the behavior of a current fed synchronous machine drive without DC-link inductance," *IEEE Trans. Power Electron.*, vol. 5, no. 2, pp. 246–251, Apr. 1990.

Velimir Nedić (S'99–M'03) was born in Belgrade, Serbia. He received the B.E.E. and M.S.E.E. degrees from the University of Belgrade, Belgrade, Serbia, in 1995 and 1998, respectively, and the Ph.D. degree in electrical engineering from the University of Wisconsin, Madison, in 2002.

Since 1995, he has been involved in various power conversion projects, with, among others, the Electrical Institute "Nikola Tesla" in Belgrade, International Rectifier Corporation, and the U.S. Air Force. He is currently with Ancra International serving as a Lead Systems Engineer for aircraft cargo power drive systems. His main interests are electronic circuits and electromechanical systems utilized in power conversion and processing.

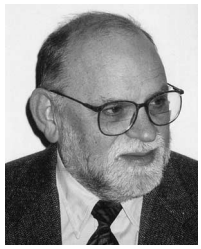

Thomas A. Lipo (M'64–SM'71–F'87) was born in Milwaukee, WI. He received the B.E.E. and M.S.E.E. degrees from Marquette University Milwaukee, WI, in 1962 and 1964, respectively, and the Ph.D. degree in electrical engineering from the University of Wisconsin, Madison, in 1968.

From 1969 to 1979, he was an Electrical Engineer in the Power Electronics Laboratory of Corporate Research and Development of the General Electric Company, Schenectady, NY. He became a Professor of electrical engineering at Purdue University, West Lafayette, IN, in 1979, and in 1981, he joined the University of Wisconsin, Madison, in the same capacity, where he is presently the W. W. Grainger Professor for Power Electronics and Electrical Machines.

Dr. Lipo has received the Outstanding Achievement Award from the IEEE Industry Applications Society, the William E. Newell Award of the IEEE Power Electronics Society, and the 1995 Nicola Tesla IEEE Field Award from the IEEE Power Engineering Society for his work. He has served IEEE in various capacities, including President of the IEEE Industry Applications Society. He is a Fellow of the Institution of Electrical Engineers, U.K., a member of the Institute of Electrical Engineers of Japan, and a Fellow of the Royal Academy of Great Britain.